

Design optimization and test campaign of a 1/50th ARIANE 5 representative dynamic model subjected to blast waves

Cédric Thémiot, Vincent Le Gallo** and Jean-Marc Carrat***

** ONERA, The French Aerospace Lab, Châtillon, France
cedric.themiot@onera.fr*

*** Airbus Safran Launchers (ASL), Les Mureaux, France
vincent.le-gallo@airbusafran-launchers.com*

Abstract

In order for CNES and Airbus Safran Launchers (ASL) to better understand the effects of the Ariane 5 lift-off blast wave, a test campaign was conducted by ONERA at Martel test bench (Poitiers, France) using a 1/50th scale mock-up equipped to characterize both the blast wave and the dynamic response of the structure. Mock-up characteristics had been optimized using Nastran to represent the dynamic behaviour of the launcher and to maximize lateral response. The FEM has been updated to match laboratory test results, and ASL was able to compare its numerical predictions with experimental results.

1 Introduction

It has been observed during several Ariane 5 lift-offs that payloads are subjected to Quasi-Static Loads (QSL), generating significant levels in the lateral direction. Therefore CNES initiated a study to simulate the effects of the blast wave hitting Ariane 5 launcher (and impacting payloads comfort) during lift-off, in order to better understand physical phenomena and enhance existing numerical models and calculation methods. This work should be helpful in the near future to predict the behaviour of Ariane 6 launcher and to verify that dynamic responses of payloads remain within specifications.

2 Objectives, similarities and preliminary design

2.1 Similarities and preliminary design of the model

The test bench used to simulate blast waves is the Pprime Institute Martel test bench in Poitiers (France). Considering the dimensional characteristics of the blast wave simulated by the bench, the scale of the representative mock-up has been set to approximately 1/50th ($\alpha=0.02$).

Hence, a similarity approach leads to a height of 1m for the model, a diameter of 108mm, and eigenfrequencies 50 times higher than those measured on the launcher.

Theoretically, keeping the original equivalent thicknesses would produce the same lateral payload QSL and would lead to high mass values inside the model. In order to maximize the payload QSL and get lower mass values, a factor $\beta=0.25$ was added to the thickness value of the 4mm thick liquid oxygen (LOX) tank. Hence, thickness of the external cylinder was set to 1mm, with the objective of maximizing dynamic response while coping with manufacturing constraints. The final value was an output of the optimization study.

Similarity relations that were used are [1] [2]:

- Length : $L_{model} = \alpha L_{launcher}$ (1)

- Diameter : $\phi_{model} = \alpha \phi_{launcher}$ (2)

- Thickness : $t_{model} = \beta t_{launcher}$ (3)

- Mass : $M_{model} = (\beta \alpha^2) M_{launcher}$ (4)

- QSL : $QSL_{model} = \beta^{-1} QSL_{launcher}$ (5)

- Eigenfrequencies : $f_{model} = \alpha^{-1} f_{launcher}$ (6)

These relations allowed having a preliminary sizing of the model and its inner components, especially (see Figure 1):

- masses of the launcher compartments: liquid hydrogen (LH2), liquid oxygen (LOX), upper cryogenic stage (ESC)
- masses of the payloads (PL) : lower payload (LPL) and upper payload (UPL).

Positions of elements were derived from their respective centre of gravity positions in real launcher configuration. Once the different target masses were initialized, potential materials (and their density) variations were derived to define an allowable space domain for model optimization. Aluminium, steel and bronze were chosen.

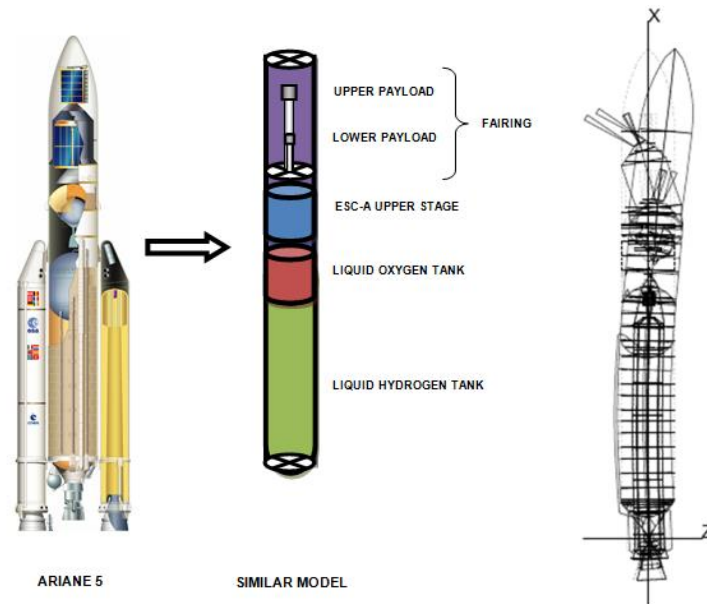


Figure 1 – ARIANE 5 launcher (left), main elements of the dynamic model (center) and one mode (right)

2.2 Test objectives and main steps

The main purpose of the model and of the Martel test campaign is the characterization of the lateral QSL of ARIANE 5 launcher in double payload configuration, responding to the lift-off blast wave excitation. The following steps were necessary to achieve this objective.

1. Characterization of the blast wave hitting the model at the Martel test bench [3]
2. Design optimization of the model to match the targeted natural modes
3. Detailed design, manufacturing and instrumentation of the model
4. Dynamic characterization and adjustment of the model with laboratory tests
5. Test campaign at Martel test bench, to measure the pressure field due to the blast wave impact on the model and the resulting dynamic response
6. Adjustment of the Finite Element Model (FEM) to match experimental results

3 Characterization of the blast wave hitting the model at the Martel test bench

A preliminary test campaign has been performed using a rigid mock-up with the same geometry as the dynamic model. Instrumentation included many more microphones than what was planned on the dynamic model [4]. Microphones were placed at 5 different altitudes along the model, with 4 or 8 microphones for each altitude distributed with a 90° (respectively 45°) azimuthal angle step.

The blast wave is the sum of two waves coming from different locations: the Ignition Over Pressure (IOP), coming directly from the engine, and the Duct Over Pressure (DOP), coming back from the exhaust ducts that exist in Kourou launch pad. A goal was to be able to isolate one of these waves to better understand their influence.

In Martel test hall, shields made of glass wool were used, installed at two different locations, in order to isolate the DOP or the IOP.

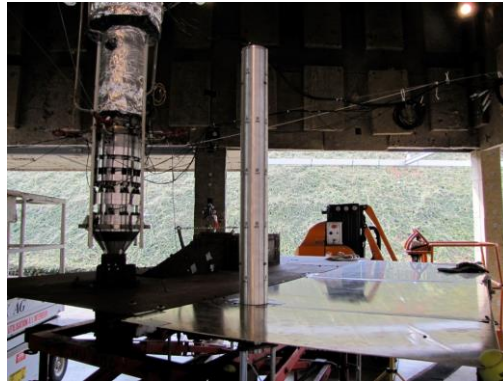


Figure 2 – Preliminary blast wave characterization test campaign

This campaign had two main objectives:

1. Identify the best location for the model for all configurations (DOP only, IOP only, DOP + IOP). Since most of QSL are due to the DOP on scale 1 launcher, the chosen location was driven by the quality of the DOP measurements.
2. Characterize the blast wave with a detailed instrumentation. Doing so, the dynamic model that includes fewer microphones on the cylinder will reuse these measurements to derive the blast waves excitation.

For the actual test campaign, the model was located at the exact chosen location, and the same glass wool shields have been used to isolate the IOP and DOP.

4 Model design optimization

The scale of the dynamic model has been chosen to fit with the dimensions of the Martel test bench. Other specifications of the model (dimensions of the inner structure, mass and material of all internal elements...) had to be determined to match the dynamic behaviour of the actual launcher as accurately as possible. An optimisation calculation has been performed by ONERA using MSC Nastran, with optimisation targets on the modal behaviour of the model including the payloads, taking into account the first four modes (eigenfrequencies and mode shapes).

4.1 Model general architecture

Based on these elements, ONERA has defined a mock-up architecture, visible in Figure 3. The objective of the calculations is then to determine the optimal characteristics of the various elements constituting the model.

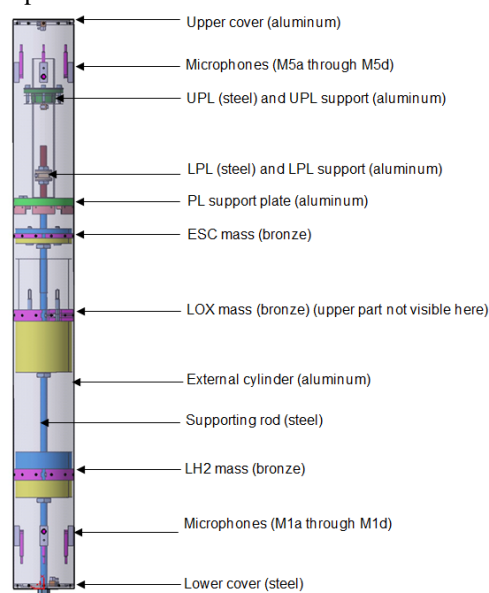


Figure 3 – Main inner elements of the dynamic model

4.2 Targeted eigenfrequencies and mode shapes

The three targeted eigenfrequencies and mode shapes are illustrated in Figure 4. From this data, relevant mode shape information was extracted for the eight strategic points. In the frequency range of interest, a non-targeted mode is present in the real launcher and in the model. This mode – number 3 – is written in italic. It was taken into account during the study and within the optimization process to avoid any coupling of this mode with others. In this paper, numbering of modes will be done according to the figure and table below.

Table 1 – List of modes in the frequency range of interest

Mode number	Mode shape
1	First cylinder bending coupled with UPL (same direction)
2	First cylinder bending coupled with UPL (opposite direction)
3	<i>Second cylinder bending</i>
4	Fairing coupled with LPL (opposite direction)

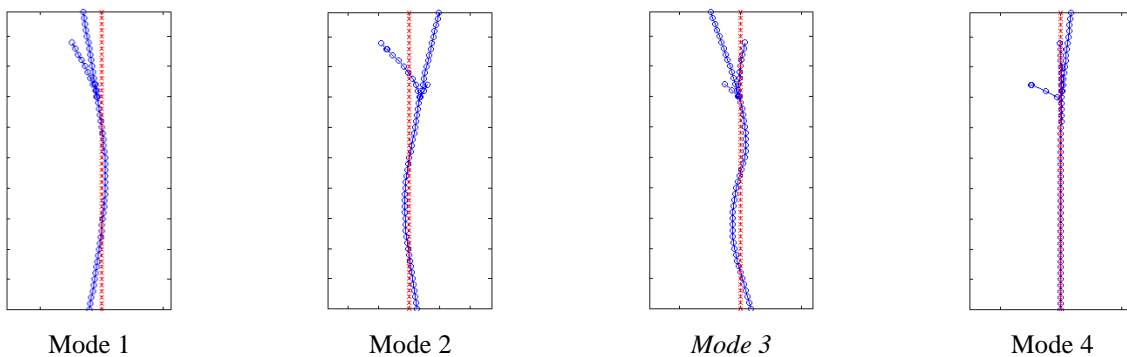


Figure 4 – Targeted eigenfrequencies and eigenmodes

The optimization process is based on ratios between the targeted and the obtained values. Attention must be paid to the relative weight of each mode contribution in the process. In order to be able to use the mode shapes in a relevant way in the optimization calculation, they have been normalized. Arbitrarily, it has been chosen to set to 1 the top cover deformation value for every mode. The generalized mass was calculated accordingly by Nastran with this assumption.

4.3 FEM of the dynamic model used in the optimization process

FEM has been generated using MSC Patran/Nastran software suite [1]. It contains 0D, 1D and 2D elements in order to be compatible with the SOL200 optimization solution [6]. Instrumentation (microphones and accelerometers) has been taken into account when masses could influence the results, typically on the external cylinder and on the covers. It was not considered for payloads since it was planned to add adjustment mass washers at these locations during the experimental characterization and adjustment process.

The LPL is fixed to a rod while the UPL is fixed to a cylinder surrounding the LPL sub-assembly.

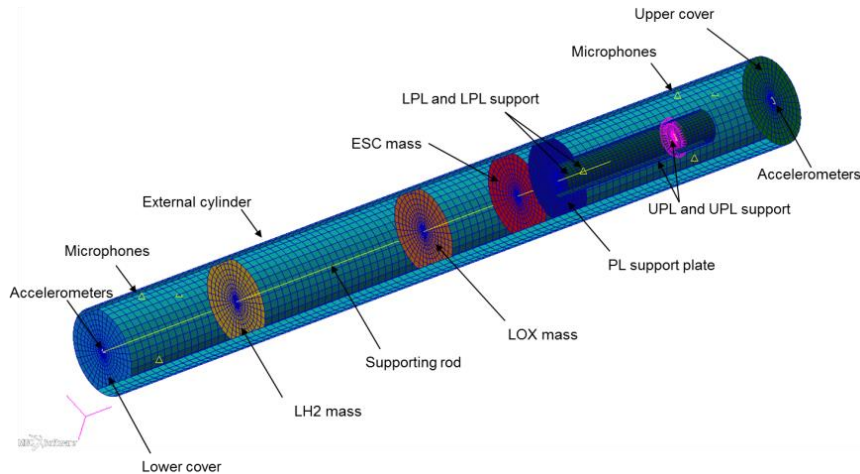


Figure 5 – FEM (MSC Patran) of the dynamic model (3/4th of the cylinder for internal vision)

4.4 Optimization process

4.4.1 Target values and design variables

Eight strategic points have been defined along the model to be used as target values in the optimization process (see Figure 3):

- Six points on the central axis of the cylinder: Lower cover, LH2 mass, LOX mass, ESC mass, PL support plate, Upper cover
- One point for each payload (LPL and UPL)

A significant number of design variables have been considered for optimization (external cylinder thickness, masses of elements, height of PL...). Several of them were linked to each other by similitude relations.

4.4.2 Objective function

The aim of the objective function is to be the most representative of the set objectives, namely 4 targeted modal frequencies and their associated displacements (see §4.2) for 8 strategic points.

The goal is to minimize the difference between the frequency (or displacement) obtained by the calculation and the target.

Several aspects should be clarified:

- Since the architecture of the model is axisymmetric, the mode analysis will return two modes with identical frequencies for each of the targeted modes above, with orthogonal displacement directions, giving 8 modes overall. Only one mode out of each pair will be considered as a target.
- Since the FEM is perfectly axisymmetric and the calculation is done in “free-free” conditions, directions of mode shapes are randomly given by Nastran with no actual physical meaning. The only important aspect is that all pairs of modes are orthogonal. Therefore, it was decided to compare the global displacement for each target point, and not the separate lateral components of the displacement, dividing by 2 the number of targeted mode shapes with no loss of information.
- In order to ensure that one of the elements in the equation is not largely dominating the others, the equation normalizes each of the subelements. For the mode shape targets, the normalization is carried out by setting the top cover displacement to 1, both for the target and the result obtained at iteration N. Thus, the comparison of the deformed cylinder for all targeted points and modes can be made with comparable amplitudes.

The overall objective function to be minimized was chosen as follows (“disp” stands for displacement):

$$\sum_{Mode=1}^4 \left(1 - \frac{Obtained\ Frequency}{Target\ Frequency}\right)^2 + \sum_{Mode=1}^4 \left(\sum_{Point=1}^8 \left(1 - \frac{Obtained\ disp\ of\ point}{Target\ disp\ of\ point}\right)^2 \right) \rightarrow 0 \quad (7)$$

It was stated that the priority should be set on mode shapes rather than eigenfrequencies. (7) shows that, for each mode, 8 elements refer to the mode shapes while only one refers to the frequency, which is in line with this priority. Several calculations were carried out adding weighting coefficients to some terms of the function (on frequencies, mode shapes, one mode compared to another...), in order to study the effects on the results. At the end, it could be observed that leaving the objective function without weighting coefficients led to satisfactory results.

4.4.3 Results of the optimization process

The main driving parameter of the calculation is the cylinder thickness, due to all the design variables that are linked to it by similitude relations. In order to lighten the model and maximize the measured dynamic responses, this thickness had to be less or equal to 1mm. Also, due to mechanical constraints, assembly risks and manufacturing difficulties, it has been agreed that it should be at least 0.5mm. A buckling analysis was performed based on aerodynamic loads estimations using a 0.5mm cylinder. No risk was identified.

In order to keep the cylinder material easily available off the shelf for a given thickness, calculations have been performed fixing the thickness value to 0.5, 0.8 and 1mm and leaving other variables as output. Optimization results were compared. Also, calculations were performed with and without instrumentation to see its impact on the cylinder deformation, especially for the thinner values. After this process, a thickness of 1mm was finally retained.

A comparison between the targeted mode shapes and the output of the optimization process can be seen on Figure 6.

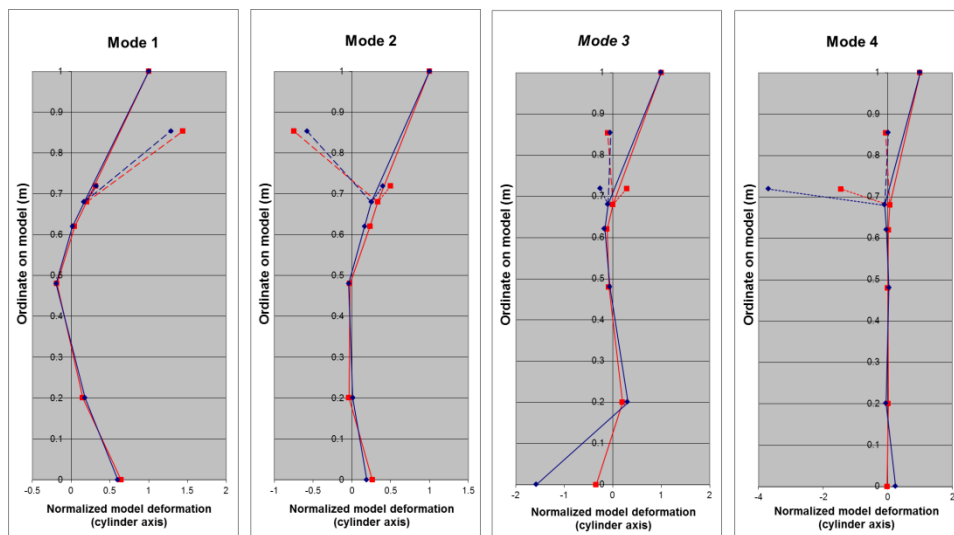


Figure 6 – Comparison between targeted mode shapes (red) and optimization results (blue)

- Modes 1 and 2 were very satisfactory.
- Mode 3 is displayed for information only. LPL direction has a comparable magnitude but in opposite direction. Lower cover has a higher magnitude, which is not a concern.
- Mode 4 was also satisfactory. It showed a higher LPL displacement than the target. The positive aspect was that it could actually help measuring this displacement.

A comparison between targeted eigenfrequencies and optimization results is shown in Figure 7.

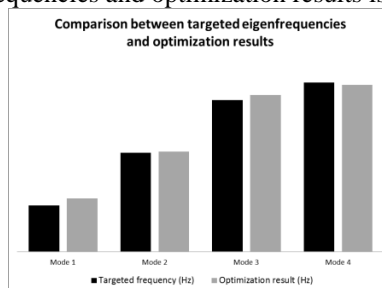


Figure 7 – Comparison between targeted eigenfrequencies (black) and optimization results (grey)

Considering that the priority of the optimization was to match the mode shapes, these results were all considered satisfactory, even mode 1 for which the frequency is the most shifted. The main goal was to keep sufficiently distant frequencies to avoid modal interaction.

4.5 Adjustment possibilities

Several calculations have been carried out with MSC Nastran using slight variations in the FEM, in order to predict how the model eigenfrequencies could be altered through adjustments that were planned during the detailed design stage. Two possibilities were considered:

- Modification of the payloads location on their support
- Modification of the payloads weight

Results allowed comparing the model sensitivity to each method. It appeared that modifying the payloads location led to more significant changes in the model eigenfrequencies, while mass adjusting could be considered for fine tuning.

5 Model instrumentation

The model included microphones on the cylinder to measure the blast wave, and accelerometers in its inner structure to characterize the dynamic response.

Two series of four microphones were installed at two levels on the model (upper and lower, see Figure 3) distributed with a 90° azimuthal angle step, noted Mia to Mid (“i” referring to the level and “a” to “d” to the azimuthal angle, see Figure 8). Those levels were already instrumented on the preliminary mock-up that had been tested earlier (see §3).

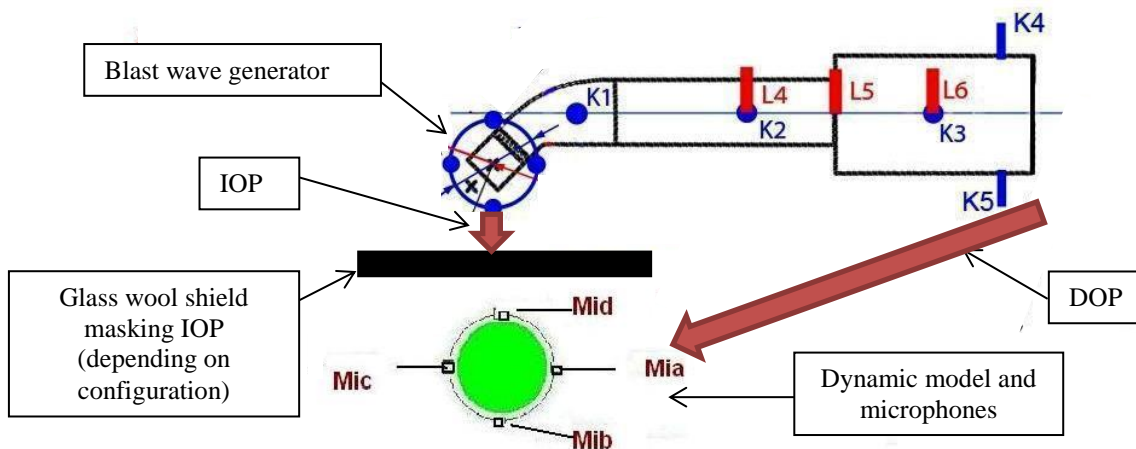


Figure 8 – Top view of the Martel test setup, illustrating microphones location

Sixteen accelerometer signals were measured inside the dynamic model:

- Two tri-axial accelerometers on the covers
- Two accelerometers to measure lateral displacements at each following level: UPL, LPL, PL support plate, LOX mass, LH2 mass

6 Modal analysis

Once the dynamic model was assembled, tests were carried out by ONERA in its laboratories to characterize the model dynamic behaviour, and if necessary to adjust the model accordingly. The following aspects were assessed: modal eigenfrequencies, shapes and damping, quality of measurements, non-linearity, and sensitivity to the payloads location.

The model was held on both ends by metal cables to simulate « free-free » conditions. The excitation system was either a hammer (for hammer tests) or a small shaker (for random, stepped sine or sweep runs).



Figure 9 – Suspension and shaker during the laboratory tests

The FRFs below were obtained using LMS Test Lab, with random excitation in the range 0-800Hz.

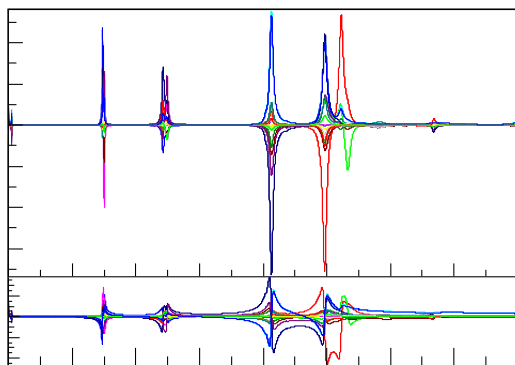


Figure 10 – FRF with imaginary (top) and real (bottom) parts

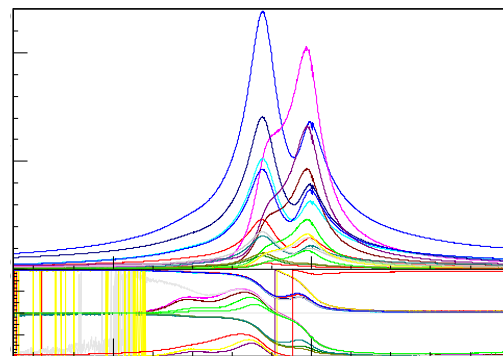


Figure 11 – FRF centered on mode 1 (double modes), amplitude (top) / phase (bottom)

One of the aspects that were foreseen in the theoretical study was that we would have to deal with orthogonal “double modes”. While theoretically identical, it was expected they would be slightly different on the manufactured model. This behavior has been identified in the laboratory tests, as seen for example in Figure 11 where the frequency range has been zoomed around the first mode. Both modes are clearly visible, with close eigenfrequencies.

This shows that the orientation of the model in Martel test hall could have some impact on the measured signals as the blast wave hits in one specific direction.

To be more precise, the blue line shows the response of the upper cover accelerometer in X direction, and the purple line the upper cover accelerometer in the Y direction. Turning the model would lead to a different distribution of the overall magnitude of the mode response between the two accelerometers.

It was therefore decided to do test runs for two azimuthal directions of the model during the Martel test campaign, one being the direction of the preliminary blast wave characterization test campaign, in order to have the microphones located the same way for these runs.

Note: for the final update of the FEM, only one of the double modes and the overall magnitudes of displacements were considered for the chosen target points, as the FEM did not take into account these slightly non-axisymmetric properties.

A MAC factor was calculated between Nastran optimization calculations and experimental data (see Figure 12) [7]. All values are above 0.8 which is satisfactory.

$$MAC(\text{exp}, \text{Nastran})_{i,j} = \frac{|\phi_{\text{exp}j}^T \cdot \phi_{\text{Nastran}j}|^2}{(\phi_{\text{exp}j}^T \cdot \phi_{\text{exp}j}) \cdot (\phi_{\text{Nastran}j}^T \cdot \phi_{\text{Nastran}j})} \quad (8)$$

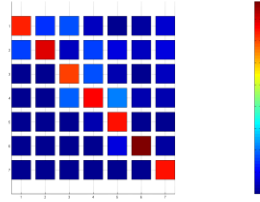


Figure 12 – MAC between Nastran optimization calculations and experimental data

Eigenfrequencies measured experimentally on the final configuration of the model are listed in Figure 13, along with initial target and Nastran optimization eigenfrequencies.

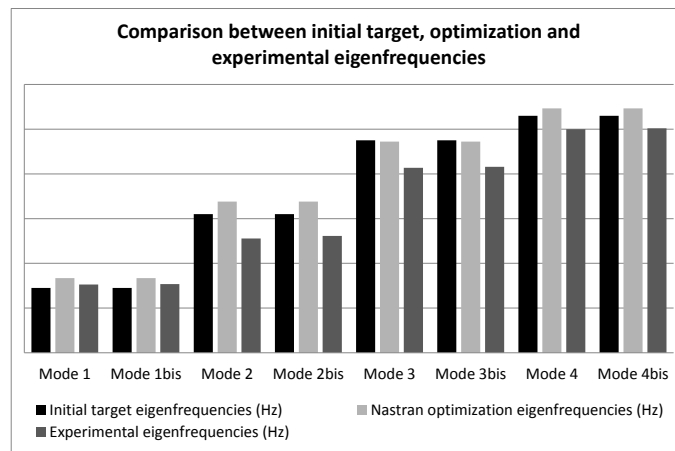


Figure 13 – Comparison between initial target, optimization and experimental eigenfrequencies

Some discrepancies can be observed, especially for mode 2 (mode 3 is irrelevant). It was possible to increase mode 2 eigenfrequency, but leading also to increase mode 1 (both are linked to UPL height) which was already above the initial target. Since the main objective of the model was on mode shapes and avoiding modal interaction, these results were the best compromise and were considered satisfactory.

Mode shapes for the strategic points of the model are shown in Figure 14. It allows comparing initial targets, Nastran optimization and experimental results. The experimental ones are close to the optimization results. Manufacturing and characterization of the model was therefore satisfactory.

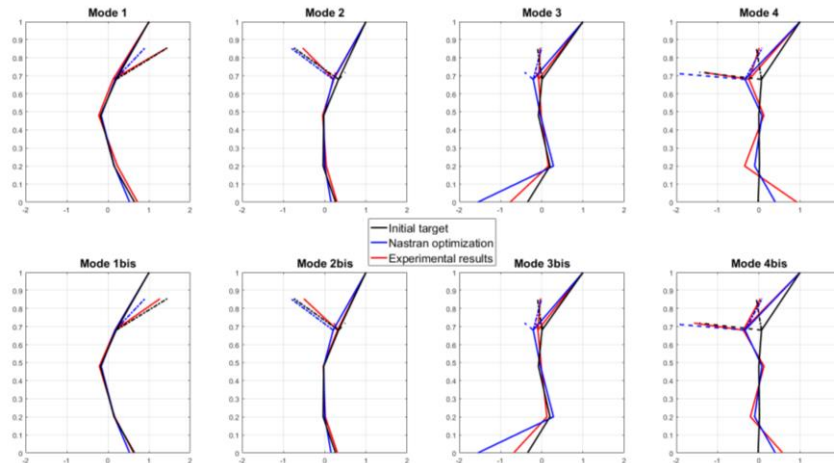


Figure 14 – Comparison of normalized mode shapes of the model

7 Update of the FEM to match experimental results

New optimization calculations have been performed by ONERA, replacing the initial targeted values by experimental laboratory results (see §6), both on frequency and mode shapes. The first results did not give full satisfaction; therefore six new design variables were added: Young moduli and densities of the three materials of the FEM. Different results were obtained depending on the boundaries assigned to each variable. Balance was to be found between getting closer to experimental results and keeping close enough to the actual geometry and properties of the model.

At the end, the updated FEM had very similar mode shapes, eigenfrequencies within $\pm 5\%$, with realistic properties.

8 Test campaign at Martel test bench

8.1 Dynamic model setup

The dynamic model was suspended from the bench ceiling and fixed to the floor (see Figure 15). A winch was used to hang the suspension cable and adjust the tension in the cables. Three straps were also installed radially at the bottom cover of the model to keep it in position and ensure its angular positioning with respect to the blast wave generator (see Figure 16).

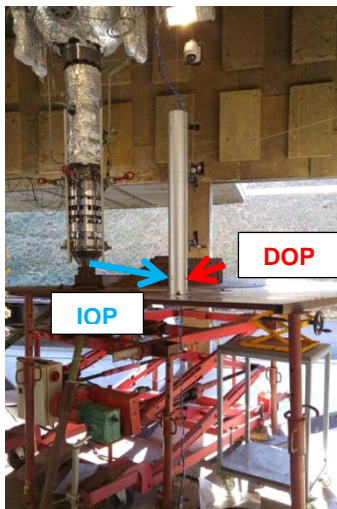


Figure 15 – Dynamic model in test hall, full blast wave DOP+IOP configuration



Figure 16 – Azimuthal control of the model

A short dynamic characterization was realized, in order to check that the results were similar to those measured during the laboratory tests, which was the case (frequency deviation less than 1%).

8.2 Test program and blast wave specific setups

In Martel test hall, shields made of glass wool were used, installed at two different locations, in order to isolate the DOP or the IOP excitation.

Ten blast wave hits were performed, to characterize the type of blast wave, and for two model azimuthal angles (0 and 30°). Two repeatability tests were performed each time.

The test program can be seen below. Each blast wave hit was named mes1, mes2, etc.

Table 2 – Test program of the Martel campaign

- | | |
|--|---|
| • Mes1, Mes2: Full blast wave, model angle 0° | • Mes7, Mes8: DOP only, model angle 0° |
| • Mes3, Mes4: Full blast wave, model angle 30° | • Mes9, Mes10: IOP only, model angle 0° |
| • Mes5, Mes6: DOP only, model angle 30° | |

An example of test results can be seen in Figure 17, where the timescale has been limited to what happens right after the blast wave (generator pressure increase and fluctuations can be seen in purple). Time response of one accelerometer for three blasts are superimposed (full blast wave, DOP only, IOP only). A 5000Hz low-pass filtering was applied.

DOP and IOP contributions can be clearly identified when comparing these signals (see Figure 17).¹

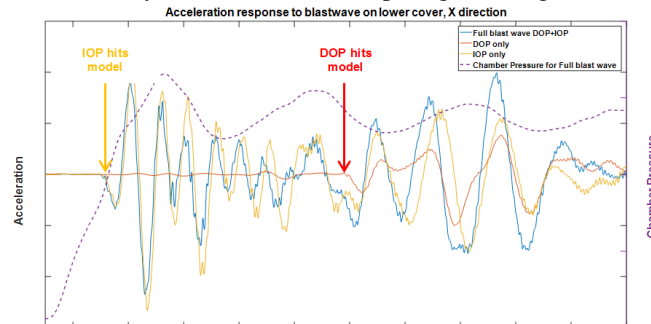


Figure 17 – Blast wave pressure rise, time response of one accelerometer, IOP and DOP participations

9 Validation of Blastwave simulation

9.1 Aerodynamic simulations

We have proceeded to the full numerical restitution of the aerodynamic blast wave produced during mes7 and repeated mes8 test. For both cases, the impact of IOP is reduced thanks to the glass wool shield.

The reference in-house aerodynamic FLUSEPA^{2TM} code is used to simulate the numerical blast-wave [8] [9]. FLUSEPA is a high order unstructured finite volume CFD code for the modeling of highly compressible, turbulent, viscous and reactive flows with particles over complex geometries in relative motion. One of the main features of FLUSEPA is its CHIMERA-like conservative overset grid method that avoids the conservation loss due to interpolation at grids intersection. It allows different geometry parts to be meshed independently and then assembled together in a single composite using a priority system and the exact geometric intersection. The aerodynamic mesh is therefore easily built with this CHIMERA-like patch technique. The overall aerodynamic domain of calculation is described in Figure 19. Especially, the cylinder and the anti-IOP shield are embedded with appropriate aerodynamic layer meshes, as can be seen in Figure 18. One can also remark that no specific model has been used to represent the glass wool acoustic absorption. A classical wall rigid no slip boundary condition was applied on the shield.

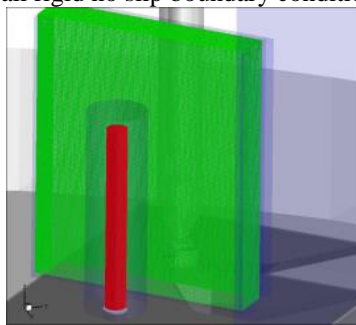


Figure 18 – CHIMERA technique

The second important feature of the simulation is its unsteady characteristic which is efficiently handled by the explicit adaptive solver of FLUSEPA. The scheme is second order consistent in time and space. Each cell can therefore progress with its maximum physical time step. A classical acceleration by a factor 10 is consequently reached.

The model takes into account the restitution of the inner experimental facility. The unsteady depressurisation of the equivalent hot gas cavity is simulated. This is the source of propulsive effect.

Phenomenology of the blast wave is described by the evolution in time of the following wall over-pressure.

¹ Timeframe shown on Figure 17 is around 20ms

² FLUSEPA French trademark N.134009261

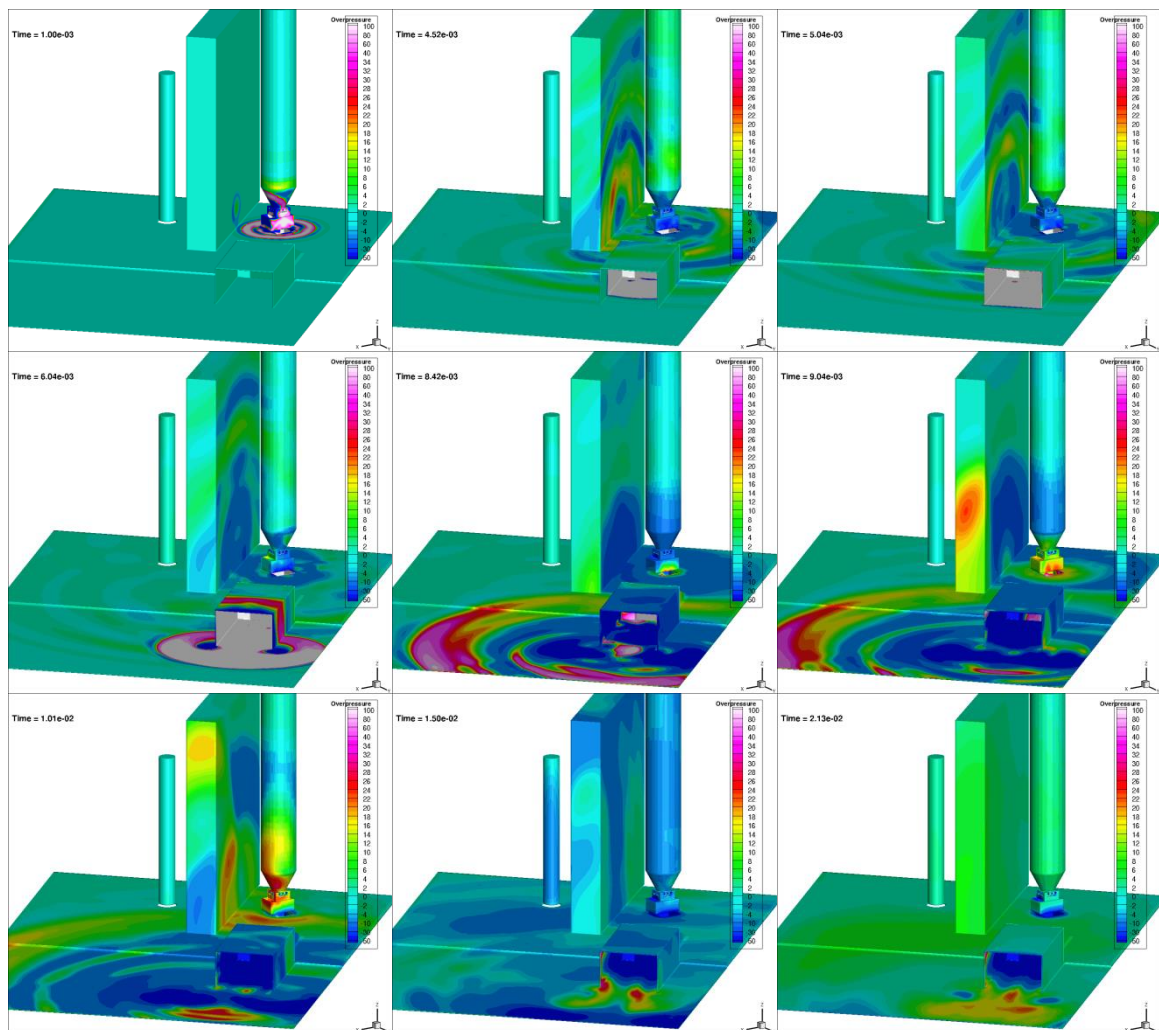


Figure 19 – Evolution of wall over-pressure – Mes7-Mes8 FLUSEPA3D simulation

Both hemispheric IOP waves, diffracted by the shield, re-joined each other behind on the cylinder. Then the inner DOP just comes out of the duct. This wave is slightly ahead in time with the outer IOP free wave. The mono-dimensional shock wave propagating in the duct is clearly a supersonic one. One can see the diffraction of the outgoing ducted over pressure wave. One can also notice at this time, the highly attenuated backward free wave, compared to the front one. The spatial directivity of the DOP wave is quite important. The pressure front coming back to the cylinder is clearly weak. One can also notice a second spurious IOP wavelet springing from the lower generator part. Meanwhile, a rarefaction wave propagates back down the duct. Later, the spurious IOP is blocked by the shield. We notice that the spurious IOP wave is synchronized with the DOP one. Without the shield, its over-pressure front would add to this latter. The DOP wave hits first the cylinder base. Besides, considering only the DOP wave, one can remark that the shield, because of its geometrical configuration, acts as a symmetry plan, and therefore does not deteriorate the DOP signal on the cylinder. At this time only, the propulsive gas flows out of the duct, in a non-coherent way and therefore does not produce any blast wave. At the end, this latter blurred pressure signal hits the cylinder.

The next figures precise the evolutions in time of the over-pressure at the various experimental probes on both rings, compared to simulated one. All this temporal signals are filtered with the same 5000 Hz calibrated low-pass filter. The M1x and M5x probes correspond respectively to the lower and the upper ring.

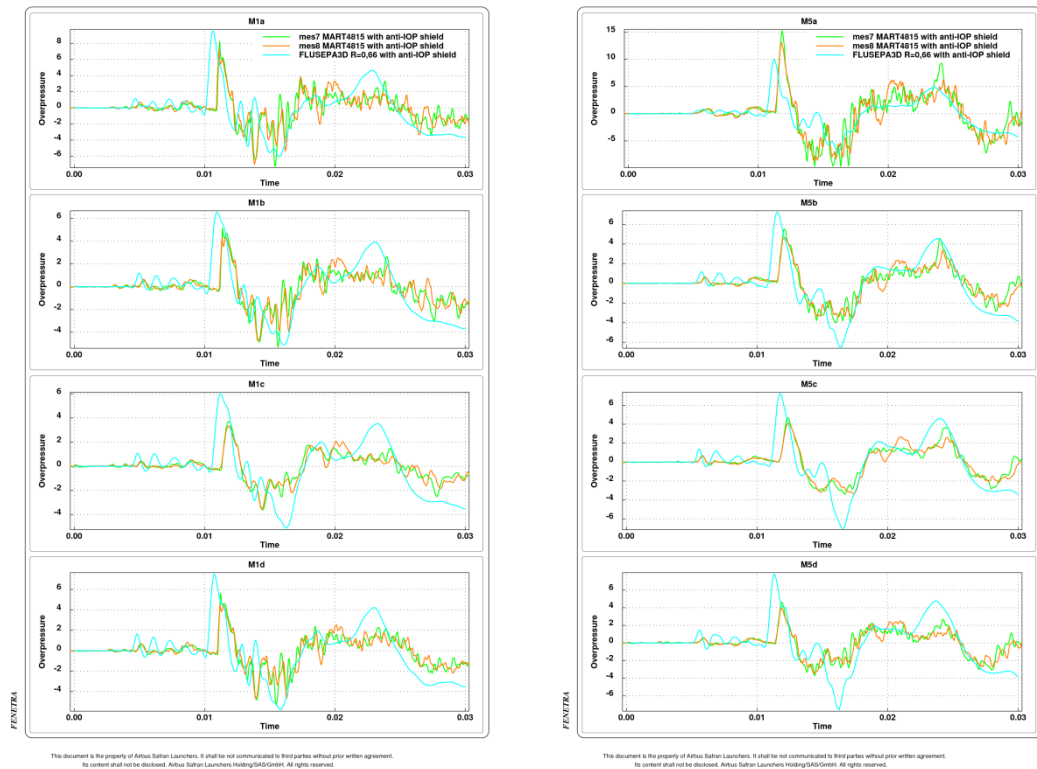


Figure 20 – MARTEL4815 dynamic mock-up campaign – Comparison FLUSEPA3D simulation and Mes7 Mes8 test fires

The general shape of the numerical curves fits well with the experimental ones. One can clearly observe the first IOP oscillations and the main DOP peak, followed by the rarefaction wave. All the temporal signals fully confirm the presence of an IOP signal in the experiment results as well as in the numerical ones. The shield does not play all its part. The IOP residual levels are nonetheless very low. The simulated IOP levels are quite higher than the experimental ones, and above all, with a frequency range content too low.

A mishap is visible on the front M5a experimental probe on the top ring. Its DOP peak level is higher than the simulated one, whereas, it is the opposite for all other probes. Generally speaking, one can remark that:

- the numerical DOP peak levels are conservative compared to the experimental ones. The maximal deviation is around twice higher, especially on the shield side probes. One can incriminate the fully reflecting ideal treatment of the shield boundary condition in the simulation.
- the numerical DOP peaks are slightly ahead compared to experimental ones.
- the attenuation of the DOP peaks with altitude is not present in the simulation and in the experiment, which is a consequence of the absence of the IOP part in the cylinder pressure signal.

Finally, the Fluid Structure Interaction analysis is done thanks to a one way coupling process. To do so, a node to node surface pressure interpolation from the aerodynamics CFD mesh to the structural cylinder one has been set up (cf. §9.2.2).

9.2 Structural dynamic simulations

9.2.1 Based on experimental pressure field

The pressure field measured during Martel test campaigns has been interpolated and projected by ASL on the external surfaces of the dynamic mock-up FEM previously updated by ONERA to fit experimental data. Then, structural dynamic simulations have been performed using PERMAS code and considering free-free representative boundary conditions.

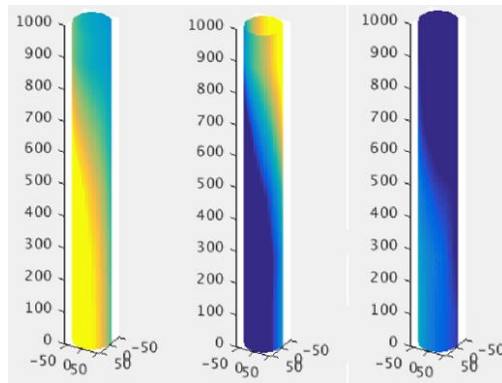


Figure 21 – Time history of the measured pressure field projected on the mock-up FEM

Based on this measured pressure field, structural dynamic simulations were very satisfactory with a very good assessment of upper and lower payloads dynamic environments (accelerations, representative of QSL), in terms of level, time history and spectra with a maximum discrepancy around 20% on maximum levels.

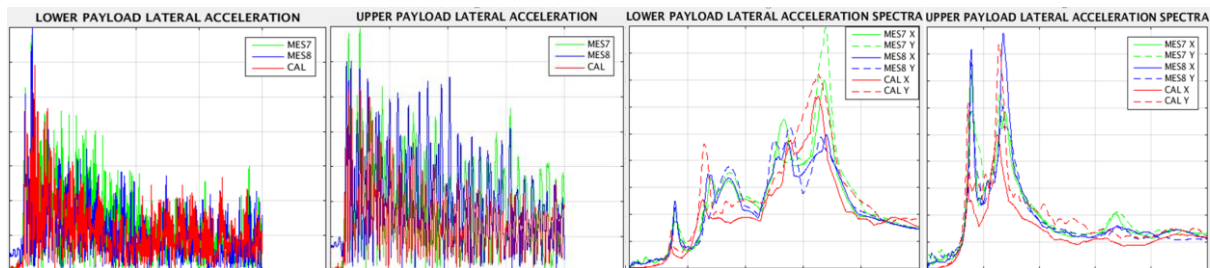


Figure 22 – Time history and spectra of the payload vibrations simulated based on measured pressure field, compared to vibration measurements

These results demonstrated the efficiency of structural dynamic FEM and tools used by ASL to predict correctly the dynamic environment and QSL of payloads on ARIANE Launchers, based on a mastered dynamic pressure field.

9.2.2 Based on simulated pressure field

The pressure field simulated in Martel test campaigns conditions has been also interpolated and projected by ASL on the external surfaces of the same dynamic mock-up FEM previously updated by ONERA. Then, structural dynamic simulations have also been performed in free-free conditions.

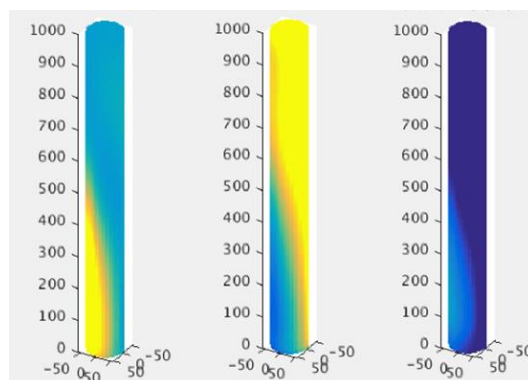


Figure 23 – Time history of the simulated pressure field projected on the mock-up FEM

Based on the simulated pressure fields, dynamic environment simulations are satisfactory with in particular a good assessment of upper payload dynamic environments, with similar time history and spectra. However, we note an over-evaluation of the lower payload dynamic environment for a particular frequency. This conservatism is due to the IOP phenomenon which has more influence in test bench conditions due to off-centering of the dynamic mock-up

from the pressure generator. This should not be the case in real lift-off conditions, as the major contributor – DOP phenomenon - is correctly predicted.

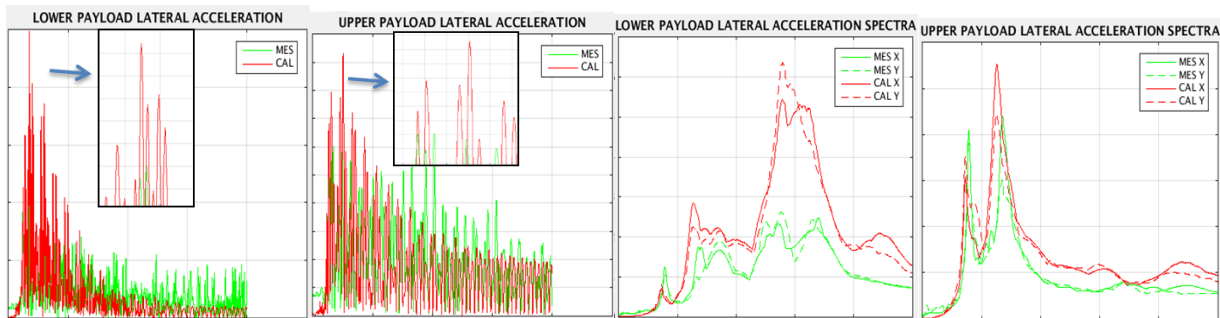


Figure 24 – Time history and spectra of the payload vibrations simulated based on simulated pressure field, compared to vibration measurements

These results pointed out a risk of conservatism associated to the IOP phenomenon, amplified by Martel test bench particular conditions (off-centering of the mock up from the gas generator). However, the DOP, major dynamic phenomenon during lift-off, should be correctly simulated on ARIANE, from aerodynamic expertise.

10 Synthesis

A test campaign has been conducted at the Martel test bench to characterize the impact of a blast wave on a flexible structure. A Nastran structural model developed and updated on experimental data by ONERA has then been used by ASL to reproduce dynamic responses. The use of measured pressures as an excitation led to consistent results whereas simulated pressures led to an overvaluation of the lower payload response for high frequencies. ASL aerodynamic analyses demonstrated that this conservatism was mainly due to IOP contribution amplified in test conditions compared to reality (off-centering of the mock-up from the blast wave generator). The DOP, which is the main phenomenon, was correctly predicted.

References

- [1] Wolowicz, C., J. Bowman, Jr., and W. Gilbert. 1979. Simitude Requirements and Scaling relationships as Applied to Model Testing.
- [2] AGARD. 1976. Destuynder R. Feasibility of dynamically similar flutter models for pressurized wind-tunnels. NASA Ames Research Center, 27-29 Sept. 1976.
- [3] Bresson, C., H. Foulon, H. Lambaré, M. Pollet, P. Malbéqui. 2011. A blast wave generator in MARTEL facility to simulate overpressure induced by solid rocket motor at lift-off. In: 4th European Conference for Aerospace Sciences, EUCASS, 4-8 July 2011, Saint-Petersburg, Russia.
- [4] Troyes, J., F. Vuillot, H. Lambaré and A. Espinosa Ramos. 2016. Numerical Study of Free Supersonic Hot Jet on Unstructured Grids with Emphasis on Aerodynamics and Resulting Radiated Noise. 22nd AIAA/CEAS Aeroacoustics Conference, May 30-June 1 2016, Lyon, France.
- [5] MSC Nastran. MSC Nastran 2012 Quick Reference Guide
- [6] MSC Nastran. MSC Nastran 2012 Design Sensitivity and Optimization User's Guide
- [7] Ewins, D.J., 2000. Modal testing : theory, practice and application (Second Edition)
- [8] Brenner, P. 1996. A Conservative Overlapping Grid to Simulate Rocket Stage Separation. 3rd Symposium on Overset Composite Grid and Solution Technology, Los Alamos. National Laboratory, New Mexico, USA, October 1996.
- [9] Pont, G., P. Brenner, P. Cinnella, J-C. Robinet and B. Maugars. 2017. Multiple-correction hybrid k-exact schemes for high-order compressible RANS-LES simulations on general unstructured grids. In: *Journal of Computational Physics*, June 2017.